Chinese Chemical Letters 34 (2023) 108594

Contents lists available at ScienceDirect

Chinese Chemical Letters

journal homepage: www.elsevier.com/locate/cclet

Supramolecular nanoparticles constructed by orthogonal assembly of pillar[5]arene-cyclodextrin dimacrocycle for chemo-photodynamic combination therapy

Yongfei Yin, Penghao Sun, Hongqiang Dong, Yi Chen, Shigui Chen*, Lu Wang*

The Institute for Advanced Studies, Wuhan University, Wuhan 430072, China

ARTICLE INFO

Article history:
Received 21 March 2023
Revised 9 May 2023
Accepted 18 May 2023
Available online 19 May 2023

Keywords:
Supramolecular nanoparticles
Host–guest systems
Photodynamic therapy
Drug delivery
Prodrugs

ABSTRACT

Chemotherapy combined with photodynamic therapy has emerged as a promising strategy for cancer treatment. However, simultaneously delivering chemotherapeutic drugs and photosensitizers and precisely adjusting the ratio of the two components as needed remains a challengeable task. Herein, novel supramolecular nanoparticles (donated as BODIPY-CPT-NPs) for chemo-photodynamic combination cancer therapy are constructed from a glutathione-responsive camptothecin-based prodrug, BODIPY photosensitizer, and dimacrocyclic host molecule through orthogonal host-guest recognitions and co-assembly. With this strategy, the ratio of prodrugs and photosensitizers in nanoparticles can be easily and precisely controlled as needed. Benefiting from the strong host-guest interactions and stable self-assembly, the nanoparticles exhibit excellent stability and photobleaching resistance. Furthermore, camptothecin can be released from nanoparticles for chemotherapy in the presence of reduction agent and single oxygen can be efficiently generated for PDT with light irradiation. The combined effects of the BODIPY-CPT-NPs have been verified in CT26 and HeLa cancer cells.

Chemotherapy is still the most common cancer treatment modality in clinics [1]. However, owing to the disadvantages such as poor water solubility [2], non-specificity [3], and serious side effects of chemotherapy drugs [4,5], the effect of chemotherapy is often unsatisfactory. In order to curb tumors effectively, besides traditional chemotherapy, a series of treatment methods have been developed by researchers [6–12]. Among them, photodynamic therapy (PDT) has been extensively studied due to its spatiotemporal selectivity, minimal invasiveness, and effectiveness [13–15]. PDT kills cancer cells mainly through reactive oxygen species (ROS) generated by photosensitizers (PSs) under light irradiation. However, the poor solubility and stability of PSs as well as the hypoxic environment of tumor tissues severely limit the further development of PDT [16,17]. Since each treatment strategy has its shortcomings, it is difficult to achieve effective suppression of malignant tumors with monotherapy. To address this dilemma, chemo-photodynamic combination therapy has been proposed in recent years. Compared with the monotherapy method, chemo-photodynamic combination therapy shows good complementarity of the two therapies [18–23], improving anti-tumor efficiency in clinical application [24,25].

Thus far, considerable effort has been focused on developing the co-delivery strategies of chemotherapeutic drugs and photosensitizers for chemo-photodynamic combination therapy, for example, loaded by nanocarriers (including liposomes [26], micelles [27], framework materials [28,29], and inorganic porous materials [30]), or constructing “drug-photosensitizer” agents *via* covalent linkage [31–34]. Due to the different pharmacokinetics and biodistribution of different agents in organisms, the precise control of the ratio of chemotherapeutic drugs and PSs is a crucial parameter for chemo-photodynamic combination therapy [35,36]. However, the strategies mentioned above usually lack a mechanism to precisely control the ratio of chemotherapeutic drugs and PSs.

Supramolecular chemistry based on non-covalent interactions has been gradually applied in the field of cancer nanotheranostics. Various agents could be used as building blocks of supramolecular cancer nanotheranostics, including chemotherapeutic drugs such as camptothecin (CPT) [37,38], paclitaxel (PTX) [39], doxorubicin (DOX) [40], and others as well as PSs (BODIPY [41,42], porphyrin [43,44], and phthalocyanine [45,46]). The water solubility and stability of chemotherapeutic drugs and PSs are significantly improved through supramolecular interactions [47,48]. Moreover, compared to traditional passive encapsulation and covalent con-

* Corresponding authors.
E-mail addresses: sgchen@whu.edu.cn (S. Chen), wanglu-027@whu.edu.cn (L. Wang).

https://doi.org/10.1016/j.cclet.2023.108594
1001-8417/

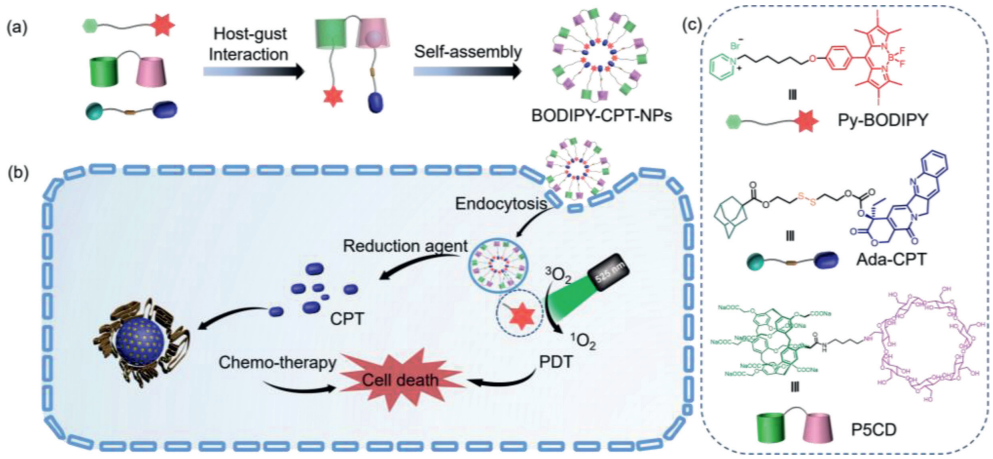

Scheme 1. (a) Preparation pathway of BODIPY-CPT-NPs *via* host-guest interactions and self-assembly; and (b) a schematic illustration of the mechanism of chemo-photodynamic combination therapy by BODIPY-CPT-NPs. (c) Chemical structures of Py-BODIPY, Ada-CPT, and P5CD.

jugation, benefitting from the dynamics and reversibility of non-covalent interactions, supramolecular cancer nanotheranostics system has excellent stimulus responsiveness, such as pH [49–51], H_2O_2 [52], glutathione (GSH) [32,53], adenosine triphosphate (ATP) [36,54,55], and enzymes [56].

Macrocyclic compounds, including cyclodextrins [57–61], cucurbiturils [62–65], calixarenes [66], and pillararenes [67–73]. Thereinto, β-cyclodextrin (β-CD) could bind to adamantane or adamantane-modified guests [74], water-soluble pillar[5]arenes (WP5) show high affinities for cationic moieties, such as pyridinium and ammonium moieties [75–77]. They all exhibit good water solubility and biocompatibility. Thus, it is possible to precisely control the ratio of chemotherapeutic drugs and PSs in supramolecular assembly, utilizing the specific recognition of prodrugs and PSs guests by the two kinds of macrocycles in the dimacrocyclic host molecule. Herein, as a proof-of-concept, we constructed a new type of supramolecular nanoparticles based on host-guest interactions for chemo-photodynamic combination therapy (Scheme 1). The supramolecular nanoparticles were composed of three components: (1) a novel dimacrocyclic host molecule (P5CD) bearing WP5 and β-CD was synthesized; (2) PSs (Py-BODIPY) decorated with pyridinium salt unit; (3) prodrug (Ada-CPT) conjugated adamantane and the chemotherapeutic drug camptothecin (CPT) by redox responsive disulfide linker. A ternary host-guest complex containing Py-BODIPY, Ada-CPT, and P5CD could be obtained through orthogonal host-guest recognitions, which then self-assembly to form supramolecular nanoparticles (BODIPY-CPT-NPs). Due to the strong host-guest interactions between WP5 of P5CD and Py-BODIPY and β-CD of P5CD and Ada-CPT, the ratio of prodrugs to PSs in the nanoparticles could be precisely adjusted as needed. As shown in Scheme 1b, after BODIPY-CPT-NPs were internalized by cancer cells, the disulfide bond of the Ada-CPT component could be reduced by the bio-reductive agent presented in the cancer cells, resulting in the release of CPT for chemotherapy, and under the irradiation of light, singlet oxygen ($^1O_2$) could be generated by the Py-BODIPY component for PDT. Cytotoxicity experiments showed that BODIPY-CPT-NPs exhibited excellent chemo-photodynamic combination therapy effects.

The dimacrocyclic host molecule P5CD, PSs Py-BODIPY, and prodrug Ada-CPT were prepared as described in Schemes S1-S3 (Supporting information). The host-guest binding behavior between WP5 of P5CD and Py-BODIPY was investigated firstly by UV-vis spectroscopy and isothermal titration calorimetry (ITC) experiments in detail. Due to the poor water solubility and photostability of Py-BODIPY, model guest (Py) was synthesized to assist in the study of the host-guest interaction between WP5 of P5CD and Py-BODIPY. As shown in Fig. S1 (Supporting information), upon stepwise addition of Py into the aqueous solution of P5CD, the absorption intensity of WP5 at 292 nm gradually increased, accompanied by an obvious bathochromic shift (Fig. S1a). An obvious inflection point appeared after the addition of 1.0 equiv. of Py (Fig. S1b), confirming the 1:1 binding stoichiometry of P5CD with Py, and the association constant between P5CD and Py was determined by nonlinear least-squares analysis to be $K_a = 3.44 \times 10^6$ L/mol (Fig. S2 in Supporting information). The binding affinity between P5CD and Py was further evaluated by ITC experiments (Fig. S3 in Supporting information). The ITC experiments for P5CD and Py suggested the 1:1 complexation and strong binding affinity ($K_a = 3.40 \times 10^6$ L/mol), which was consistent with the UV-vis titration result. It is known that β-CD could form host-guest complexes with adamantane-containing guests in a 1:1 stoichiometry with high association constant, generally reach up to 10^4 L/mol in water [78]. In addition, the optimized structure of the ternary host-guest complex formed by Py-BODIPY, Ada-CPT, and P5CD was obtained by theoretical calculation (Fig. S4 in Supporting information). These results suggested the capability of P5CD to simultaneously bind both Py-BODIPY and Ada-CPT with strong binding affinity, forming three-component supramolecular amphiphiles and then self-assembled into supramolecular nanoparticles.

Before investigating the supramolecular nanoparticles, the self-assembly behavior of free Py-BODIPY or free Ada-CPT in an aqueous solution (1.0×10^{-5} mol/L, containing 0.1% DMSO) was first investigated by dynamic light scattering (DLS). The results showed that almost no signal was detected during the experiments with free Py-BODIPY, which indicated that the free Py-BODIPY could not form effective aggregates under the experimental concentration conditions. However, the hydrophobic prodrug Ada-CPT formed large-sized aggregates (average diameter: 812.8 nm) in water (Fig. S5 in Supporting information), which may be due to the disulfide bond induced chalcogen bonding interaction and the π-π interaction of CPT [79,80]. Subsequently, BODIPY-CPT-NPs were conveniently prepared by mixing Py-BODIPY and Ada-CPT with P5CD in aqueous solution due to the strong electrostatic and hydrophobic interactions between them. For comparison purposes, Py-BODIPY-based PDT supramolecular nanoparticles (BODIPY-NPs) and Ada-CPT-based chemotherapy supramolecular nanoparticles (CPT-NPs) were prepared using the same method (Scheme 1a and Fig. 1a). The size and morphology of the three kinds of supramolecular nanoparticles were investigated by DLS, scanning electron microscopy (SEM), and transmission electron microscopy (TEM) mea-

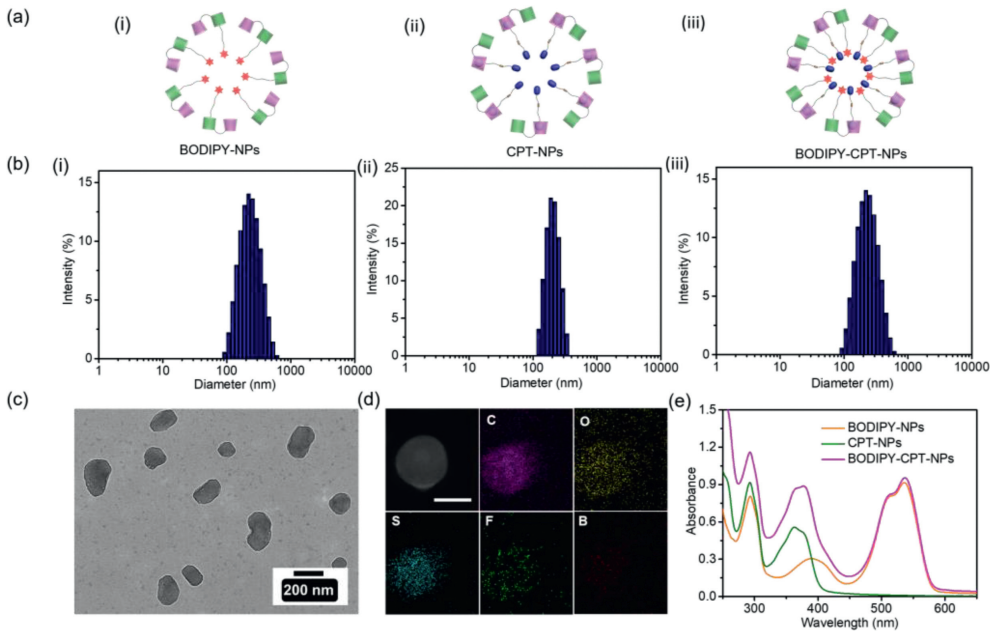

Fig. 1. (a) Schematic illustration of (i) BODIPY-NPs, (ii) CPT-NPs, and (iii) BODIPY-CPT-NPs. (b) DLS size distribution of (i) BODIPY-NPs, (ii) CPT-NPs, and (iii) BODIPY-CPT-NPs. (c) TEM images of BODIPY-CPT-NPs. (d) EDS element mapping of C, O, S, F, and B of BODIPY-CPT-NPs by HAADF-STEM image. Scale bar: 100 nm. (e) UV-vis spectra of BODIPY-NPs, CPT-NPs, and BODIPY-CPT-NPs.

surements. According to DLS results, the average hydrodynamic diameter (D_H) of BODIPY-NPs, CPT-NPs, and BODIPY-CPT-NPs were 187.6, 142.4, and 179.1 nm, respectively (Fig. 1b). SEM and TEM images clearly showed the morphology of spherical structures with diameters consistent with the DLS results (Fig. 1c, Figs. S6 and S7 in Supporting information). To further demonstrate the successful preparation of BODIPY-CPT-NPs, elemental mapping based on high-angle annular dark-field scanning TEM (HAADF-STEM) was first employed (Fig. 1d). The results showed that the featured S element from Ada-CPT was distributed uniformly throughout the entire nanoparticle. Additionally, the featured F and B element derived from Py-BODIPY could also be found in the element mapping, suggesting the predesigned structure of BODIPY-CPT-NPs. The stability of BODIPY-CPT-NPs in H_2O, phosphate-buffered saline (PBS), Dulbecco's modified Eagle's medium (DMEM), and DMEM with 10% fetal bovine serum (FBS) was investigated by detecting their D_H and polydispersibility (PDI) changes based on DLS experiments (Fig. S8 in Supporting information), while no clear change in the D_H and PDI were observed for 6 days, indicating the excellent stability of BODIPY-CPT-NPs in these four media. In addition, DLS showed that ζ-potential of BODIPY-NPs, CPT-NPs, and BODIPY-CPT-NPs were -46.7, -53.9, and -48.7 mV, respectively (Fig. S9 in Supporting information). The high negative ζ-potential of these nanoparticles could be attributed to the anion WP5 of P5CD.

The strong binding affinity and orthogonal host-guest interactions of Py-BODIPY and Ada-CPT to P5CD offer great potential for precisely controlling the ratio of PSs and prodrugs. For the demonstration, nanoparticles with different ratios of Py-BODIPY and Ada-CPT (1:5, 3:5, 5:3, and 5:1) were also prepared (Fig. S10 in Supporting information). DLS results showed that the D_H of these supramolecular nanoparticles ranged from 170.8 nm to 226.9 nm (Fig. S11 in Supporting information). TEM revealed that the morphologies of these nanoparticles were spherical (Fig. S12 in Supporting information). Furthermore, these nanoparticles were diluted from 50 μmol/L, and the changes in D_H were monitored by DLS (Fig. S13 in Supporting information). The results showed that these nanoparticles had similar D_H compared with the initial concentration condition when diluted to a concentration as low as 0.05 μmol/L, which further demonstrated that the supramolecular nanoparticles formed through host-guest interactions have excellent stability. This will be beneficial for the application in therapy systems.

The photophysical properties of BODIPY-CPT-NPs were evaluated by UV-vis spectroscopy and FL spectroscopy. As shown in Fig. 1e, the typical absorbance peaks of three components, including P5CD (292 nm), Ada-CPT (363 nm, 379 nm), and Py-BODIPY (509 nm, 536 nm) were observed in the BODIPY-CPT-NPs solution, which further confirmed the co-assembly of these three components. Interestingly, due to significant overlap between the emission spectrum of Ada-CPT and the absorption spectrum of Py-BODIPY (Fig. S14a in Supporting information), a fluorescence resonance energy transfer (FRET) effect was observed in aqueous solution of BODIPY-CPT-NPs. Upon excitation at 370 nm, the fluorescence emission of BODIPY-CPT-NPs at 437 nm was substantially quenched and was much weaker than that of free Ada-CPT and CPT-NPs (Fig. S14b in Supporting information).

Given the intramolecular FRET effect in BODIY-CPT-NPs, the release process of CPT could be monitored by fluorescence spectroscopy (Fig. 2a). Since BODIY-CPT-NPs were prone to precipitate in GSH-containing solution, dithiothreitol (DTT) was chosen as the reducing agent to cleave disulfide bonds (Fig. S16 in Supporting information). Upon the addition of DTT (10.0 mmol/L), the emission of BODIY-CPT-NPs solution at 437 nm significantly enhanced, indicating the gradual cleavage of the disulfide bonds of Ada-CPT and the release of CPT (Figs. 2b and c, as well as Fig. S15 in Supporting information). CPT release behavior of BODIY-CPT-NPs was further investigated by using high-performance liquid chromatography (HPLC). From the HPLC results (Fig. S17 in Supporting information), the retention time of free CPT and BODIY-CPT-NPs was 5.83 and 20.47 min, respectively. After incubating BODIY-CPT-NPs with DTT, a new peak corresponding to CPT was observed at 5.83 min, which was enhanced with extending incubation time and accompanied by a decrease in the peak of BODIY-CPT-NPs. Furthermore, in the presence of 1.0 mmol/L DTT, only a small amount of CPT (21.2%) was released within 3 h. In contrast, 54.8% and 92.5% of CPT was released from BODIY-CPT-NPs treated with 5.0 mmol/L

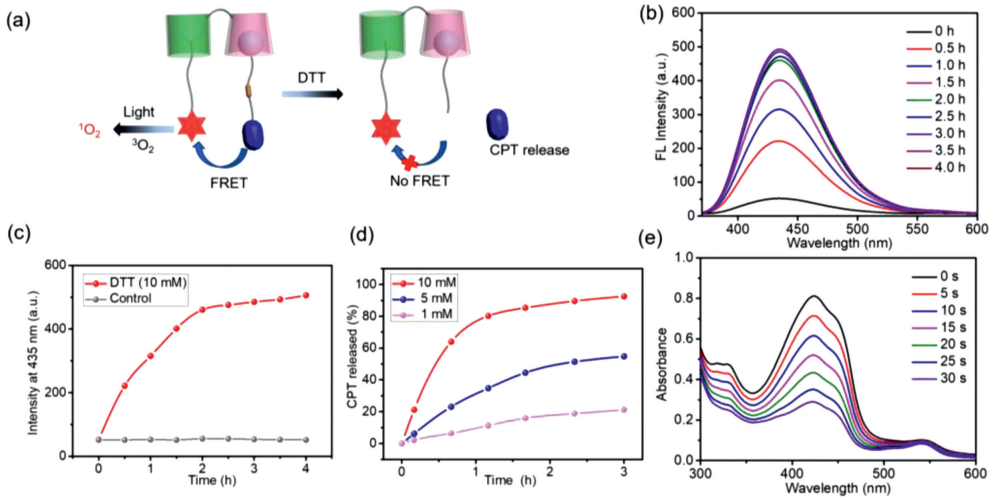

Fig. 2. (a) Schematic diagram of BODIPY-CPT-NPs releasing CPT and generating $^1O_2$ under DTT and light, respectively. (b) Fluorescence spectra of BODIPY-CPT-NPs after being incubated with DTT (10.0 mmol/L) at 37 °C for different time periods. (c) Changes of fluorescence intensity of BODIPY-CPT-NPs in the presence of DTT (10.0 mmol/L) or in the absence of DTT. (d) *In vitro* time-dependent CPT release efficiency of BODIPY-CPT-NPs in the presence of different concentrations of DTT at 37 °C. CPT concentration was determined by HPLC. (e) The generation of $^1O_2$ during the exposure of BODIPY-CPT-NPs to light (525 nm, 40 mW/cm^2) irradiation, evaluated by 1,3-diphenylisobenzofuran (DPBF)-based assays.

and 10.0 mmol/L DTT, respectively (Fig. 2d). These studies showed that the release of CPT from BODIY-CPT-NPs in the presence of DTT showed concentration-dependence, which will be beneficial to realize the rapid release of CPT from nanoparticles in cancer cells with high GSH concentration and remain stable in normal cells.

The capability of ROS production is a critical parameter to evaluate a photodynamic therapy system. The generation ability of $^1O_2$ was evaluated during the exposure of BODIPY-CPT-NPs solution to light (525 nm, 40 mW/cm^2) irradiation using 1,3-diphenylisobenzofuran (DPBF) as the indicator. DPBF could react with $^1O_2$, which resulted in decrease in its characteristic absorbance at 425 nm (Fig. S18a in Supporting information). As shown in Fig. 2e, the absorbance of the DPBF at 425 nm in the presence of the BODIPY-CPT-NPs decreased rapidly within 30 s, indicating the production of $^1O_2$. The decay rates of DPBF were comparable when compared with BODIPY-CPT-NPs, BODIPY-NPs, and Py-BODIPY (Figs. S18b-f in Supporting information), suggesting that the introduction of host-guest interactions and co-assembly with prodrug molecules did not affect the $^1O_2$ generation capability of BODIPY PSs.

PSs are known to be prone to photodegradation [81]. Thus, the photostability of BODIPY-CPT-NPs was measured by monitoring changes in the UV-vis spectra. As shown in Fig. S19 (Supporting information), after 3 h of room light exposure, the absorbance attributed BODIPY-CPT-NPs decreased slowly and the degradation rate was only 11.6%, however, BODIPY-NPs and free Py-BODIPY were photodegraded by 22.1% and 72.8%, respectively. The results showed that the photostability of BODIPY-CPT-NPs was much higher than that of free Py-BODIPY and slightly higher than that of BODIPY-NPs, which might be attributed to host-guest interactions and the formation of stable assemblies [47,82]. The excellent photostability of BODIPY-CPT-NPs facilitates material storage and durable PDT.

The cellular uptake behavior of BODIPY-CPT-NPs was studied by confocal laser scanning microscope (CLSM). CT26 cells were incubated with BODIPY-NPs, CPT-NPs, and BODIPY-CPT-NPs for 4 h, respectively. The cells were imaged by CLSM at fluorescence channels for CPT (blue) and BODIPY (red), CLSM showed that the red fluorescence in BODIPY-NPs treated CT26 cells and the blue fluorescence in CPT-NPs treated CT26 cells, while BODIPY-CPT-NPs treated CT26 cells display both blue and red fluorescence (Fig. 3a), which indicated that the supramolecular nanoparticles formed by three-component self-assembly successfully achieved the co-delivery of chemotherapeutic drugs and PSs. Finally, the $^1O_2$ generation in CT26 cells treated with BODIPY-NPs or BODIPY-CPT-NPs was detected by DCFH-DA staining. Under light irradiation, a strong green fluorescence was observed in BODIPY-NPs or BODIPY-CPT-NPs treated cells (Fig. 3b), which indicated that BODIPY-NPs or BODIPY-CPT-NPs could efficiently produce $^1O_2$ in CT26 cells under light irradiation.

Before studying the chemo-photodynamic combination therapy efficacy of BODIPY-CPT-NPs, the cytotoxicity of P5CD in the CT26 cells was first assessed using a Cell Counting Kit-8 (CCK-8) assay. P5CD exhibited negligible cytotoxicity to CT26 cells even at higher concentration (160 μmol/L) (Fig. S20 in Supporting information), showing the excellent biocompatibility. Subsequently, the cytotoxicity of Ada-CPT and CPT-NPs were studied. The cell survival rate gradually decreased with the increase of the Ada-CPT concentration (Fig. S21a in Supporting information), which indicated that overexpression GSH in the microenvironment of CT26 cancer cells led to the cleavage of disulfide bonds and the release of CPT. The dark toxicity of Py-BODIPY and BODIPY-NPs were also studied (Fig. S21b in Supporting information), the results showed that compared with Py-BODIPY, the dark toxicity of BODIPY-NPs had a certain degree of reduction, which may be attributed to the host-guest interaction between Py-BODIPY and P5CD. However, the low dark toxicity of PSs should be taken into consideration in the chemo-photodynamic combination therapy system design [83]. To minimize the undesired dark toxicity from PSs, the molar ratio of Py-BODIPY and Ada-CPT in BODIPY-CPT-NPs was controlled at 1:5 for the subsequent cell study.

Finally, the efficacy of combination therapy was evaluated. Cancer cells CT26 and HeLa were used to determine the chemo-photodynamic combination therapy effect of BODIPY-CPT-NPs. As shown in Fig. 4a, CT26 cells treated with BODIPY-CPT-NPs in the dark and BODIPY-NPs under light irradiation were used as comparisons for chemotherapy and PDT, respectively. After exposure to light irradiation (525 nm, 40 mW/cm^2, 2 min), the viability of CT26 cells treated with BODIPY-NPs decreased upon increasing PSs concentration. This result indicated that $^1O_2$ produced by BODIPY-NPs under light irradiation could effectively damage and kill cancer cells. The capacity of chemotherapy of BODIPY-CPT-NPs was

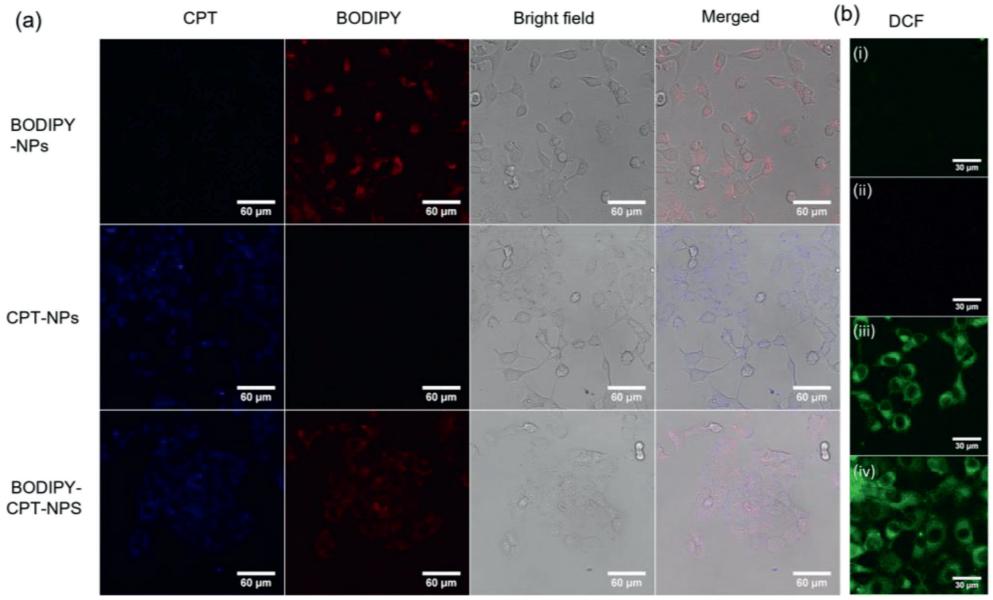

Fig. 3. (a) CLSM images of CT26 cells treated with BODIPY-NPs, CPT-NPs, and BODIPY-CPT-NPs for 4 h. The blue fluorescence signals are from CPT moieties, and red fluorescence signals are from BODIPY moieties. Scale bars: 60 μm. (b) The intracellular ROS level investigations in CT26 cells treated with BODIPY-NPs or BODIPY-CPT-NPs in the dark or in the presence of light (525 nm, 40 mW/cm^2, 2 min) through CLSM. (i) BODIPY-NPs (dark), (ii) BODIPY-CPT-NPs (dark), (iii) BODIPY -NPs (light), (iv) BODIPY-CPT-NPs (light). Scale bars: 30 μm.

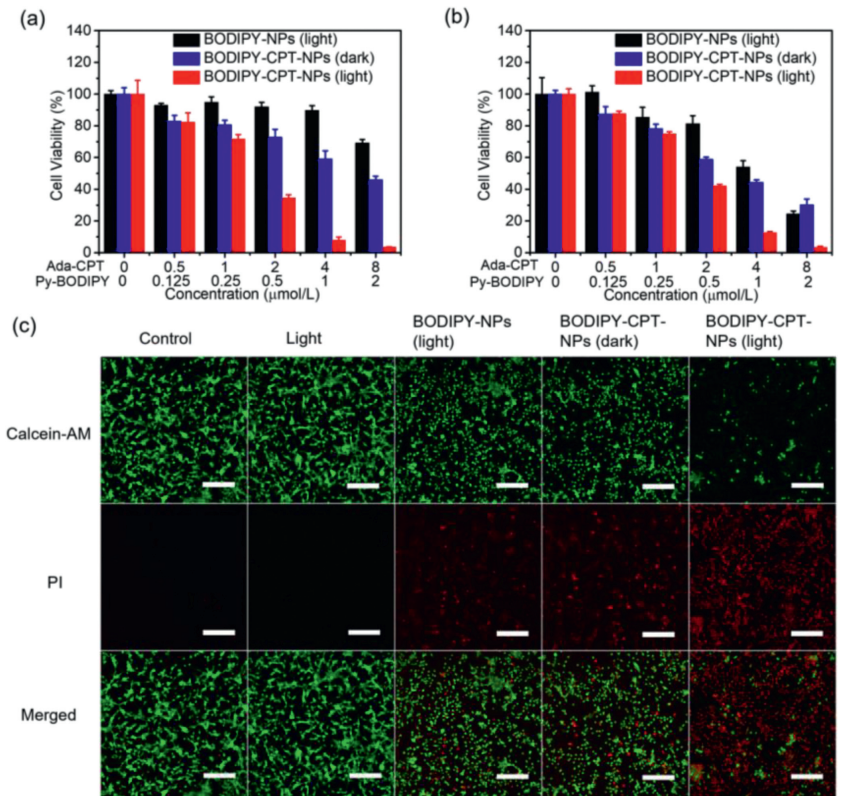

Fig. 4. *In vitro* cell viability of (a) CT26 cells and (b) HeLa cells after 24 h treatment with BODIPY-NPs or BODIPY-CPT-NPs in the absence and presence of light (525 nm, 40 mW/cm^2, 2 min). Data points represent mean ± SD ($n = 4$). (c) Confocal laser scanning microscopy images of calcein AM and propidium iodide co-staining on CT26 cells upon different treatments. Scale bars: 200 μm.

also dependent on concentration. Particularly, BODIPY-CPT-NPs under light irradiation presented the highest anticancer effect at the same prodrugs and PSs concentrations. In addition, the cytotoxicity against HeLa cells was similar to that against CT26 cells (Fig. 4b).

The combinational therapy efficacy of BODIPY-CPT-NPs was further characterized by using the live/dead cell staining assay on CT26 cells. Calcein acetoymethyl ester (calcein-AM) emits green fluorescence in living cells, and propidium iodide (PI) emits red fluorescence in dead cells. As shown in Fig. 4c, control groups of CT26 cells without any treatment in the dark or treated with light alone emitted strong green fluorescence without red fluorescence, proving that the cells survived well under these con-

ditions. In contrast, red fluorescence was observed in cells incubated with BODIPY-NPs under light and BODIPY-CPT-NPs in the dark, demonstrating the PDT effect of BODIPY-NPs under light and the chemotherapeutic effect of BODIPY-CPT-NPs in the dark. While when cells were incubated with BODIPY-CPT-NPs under light, strong red fluorescence was shown, indicating highest cytotoxicity caused by the combination of chemotherapy and PDT, which was consistent with the results of CCK-8. Taken together, the above-mentioned results suggested that the chemo-photodynamic combination therapy effect provided by BODIPY-CPT-NPs was more effective than monotherapy.

In summary, we have constructed a new type of supramolecular nanoparticles (BODIPY-CPT-NPs) for chemo-photodynamic combination therapy based on host-guest interactions between dimacrocyclic host molecule (P5CD) and two therapeutic agents. Benefiting from the orthogonal host-guest recognitions and flexible supramolecular self-assembly, the ratio of prodrug and PSs in supramolecular nanoparticles could be precisely controlled as needed. The obtained supramolecular nanoparticles showed excellent physical stability and photostability. In addition, nanoparticles can effectively generate $^1O_2$ and release the chemotherapeutic drug CPT under light irradiation and in the presence of reduction agent, respectively. *In vitro* cell experiments showed that BODIPY-CPT-NPs could be efficiently internalized by CT26 cells and had a significant combined therapeutic effect on cancer cells under light irradiation. Considering the great potential of combination therapy, this work may provide a novel approach for the construction of chemo-photodynamic combination therapy systems.

Declaration of competing interest

The authors declare that they have no known competing financial interests or personal relationships that could have appeared to influence the work reported in this paper.

Acknowledgments

This work was supported by National Natural Science Foundation of China (Nos. 21702153 and 21801194), and Wuhan Science and Technology Bureau (No. whkxjsj009). We thank the support of the Core Facility of Wuhan University and the Large-scale Instrument and Equipment Sharing Foundation of Wuhan University. We thank Prof. Suming Chen and Chunrong Liu for the support at cell experiments.

Supplementary materials

Supplementary material associated with this article can be found, in the online version, at doi:10.1016/j.cclet.2023.108594.

References

[1] V.T. DeVita Jr., E. Chu, Cancer Res. 68 (2008) 8643–8653.
[2] S. Teixeira, M.A. Carvalho, E.M.S. Castanheira, Biomedicines 10 (2022) 486.
[3] A. Wadhawan, M. Chatterjee, G. Singh, Int. J. Mol. Sci. 20 (2019) 5243.
[4] S. Wolf, D. Barton, L. Kottschade, et al., Eur. J. Cancer 44 (2008) 1507–1515.
[5] C. Bailly, Int. Immunopharmacol. 77 (2019) 105967.
[6] D. De Ruysscher, G. Niedermann, N.G. Burnet, et al., Nat. Rev. Dis. Primers 5 (2019) 13.
[7] W. Chen, C. Liu, X. Ji, et al., Angew. Chem. Int. Ed. 60 (2021) 7155–7164.
[8] P. Wust, B. Hildebrandt, G. Sreenivasa, et al., Lancet Oncol. 3 (2002) 487–497.
[9] H.S. Jung, P. Verwilst, A. Sharma, et al., Chem. Soc. Rev. 47 (2018) 2280–2297.
[10] X. Deng, Z. Shao, Y. Zhao, Adv. Sci. 8 (2021) 2002504.
[11] Q. Liu, Y. Duo, J. Fu, et al., Nano Today 36 (2021) 101023.
[12] S. Son, J. Kim, J. Kim, et al., Chem. Soc. Rev. 51 (2022) 8201–8215.
[13] J.F. Lovell, T.W.B. Liu, J. Chen, G. Zheng, Chem. Rev. 110 (2010) 2839–2857.
[14] T.J. Dougherty, Photochem. Photobiol. 58 (1993) 895–900.
[15] V.N. Nguyen, Y.X. Yan, J.Z. Zhao, J.Y. Yoon, Acc. Chem. Res. 54 (2021) 207–220.
[16] J. Pouyssegur, F. Dayan, N.M. Mazure, Nature 441 (2006) 437–443.
[17] Y.Y. Liu, Y. Liu, W.B. Bu, et al., Angew. Chem. Int. Ed. 54 (2015) 8105–8109.
[18] L. Zhang, J. Wang, Y. Zhang, et al., Dyes Pigm. 170 (2019) 107588.
[19] R. Ruiz-Gonzalez, P. Milan, R. Bresoli-Obach, et al., Cancers 9 (2017) 18.
[20] W. Mao, Y. Liao, D. Ma, Chem. Commun. 56 (2020) 4192–4195.
[21] Y. Xu, Y. Wang, J. An, et al., Bioact. Mater. 14 (2022) 76–85.
[22] Y. Wang, D. Wang, J. Wang, et al., Chem. Commun. 58 (2022) 1689–1692.
[23] J. Wang, D. Wang, M.P. Cen, et al., J. Nanobiotechnol. 20 (2022) 33.
[24] D. Liu, B. Li, W. Shi, et al., Photodiagn. Photodyn. Ther. 25 (2019) 317–318.
[25] X. Dong, Y. Zeng, Z. Zhang, et al., J. Pharm. Pharmacol. 73 (2021) 425–436.
[26] L. Feng, L. Cheng, Z. Dong, et al., ACS Nano 11 (2017) 927–937.
[27] G. Gong, J. Pan, Y. He, et al., Theranostics 12 (2022) 2028–2040.
[28] L. Zhang, Y. Gao, S. Sun, et al., J. Mater. Chem. B 8 (2020) 1739–1747.
[29] J. Chen, X. Tan, Y. Huang, et al., Biomaterials 284 (2022) 121513.
[30] E. de las Heras, M.L. Sagrista, M. Agut, S. Nonell, Pharmaceutics 14 (2022) 405.
[31] L.H. Liu, W.X. Qiu, L. Bin, et al., Adv. Funct. Mater. 26 (2016) 6257–6269.
[32] Y. Yang, Y. Zhang, R. Wang, et al., Chin. Chem. Lett. 33 (2022) 4583–4586.
[33] P. Thapa, M. Li, M. Bio, et al., J. Med. Chem. 59 (2016) 3204–3214.
[34] F. Zhang, Q. Ni, O. Jacobson, et al., Angew. Chem. Int. Ed. 57 (2018) 7066–7070.
[35] H.Z. Chen, X.W. Zeng, H.P. Tham, et al., Angew. Chem. Int. Ed. 58 (2019) 7641–7646.
[36] Z. Su, D. Xi, Y. Chen, et al., Small 19 (2023) 2205825.
[37] K. Yang, S. Qi, X. Yu, et al., Angew. Chem. Int. Ed. 61 (2022) e2022037.
[38] G. Yu, X. Zhao, J. Zhou, et al., J. Am. Chem. Soc. 140 (2018) 8005–8019.
[39] Y.J. Liu, X.H. Zheng, J.L. Zhou, Z.G. Xie, J. Mater. Chem. B 9 (2021) 2334–2340.
[40] P. Zhang, J. Wang, H. Chen, et al., J. Am. Chem. Soc. 140 (2018) 14980–14989.
[41] L.B. Meng, W.Y. Zhang, D.Q. Li, et al., Chem. Commun. 51 (2015) 14381–14384.
[42] H.B. Cheng, H. Dai, X. Tan, et al., Adv. Mater. 34 (2022) 2109111.
[43] J. Tian, B.X. Huang, Z.P. Cui, et al., Acta Biomater. 130 (2021) 447–459.
[44] Y. Liu, C.Z. Liu, Z.K. Wang, et al., Biomaterials 284 (2022) 121467.
[45] X. Li, E.Y. Park, Y. Kang, et al., Angew. Chem. Int. Ed. 59 (2020) 8630–8634.
[46] X.Y. Dai, M. Huo, B. Zhang, et al., Biomacromolecules 23 (2022) 3549–3559.
[47] K. Yang, J. Wen, S. Chao, et al., Chem. Commun. 54 (2018) 5911–5914.
[48] D. Ma, G. Hettiarachchi, N. Duc, et al., Nat. Chem. 4 (2012) 503–510.
[49] Y.C. Zhang, P.Y. Zeng, Z.Q. Ma, et al., Drug Deliv. 29 (2022) 128–137.
[50] J. Chen, Y. Zhang, Z. Meng, et al., Chem. Sci. 11 (2020) 6275–6282.
[51] W. Li, S. Yin, Y. Shen, et al., J. Am. Chem. Soc. 145 (2023) 3736–3747.
[52] Z.Y. Shen, N. Ma, F. Wang, et al., Chin. Chem. Lett. 33 (2022) 4563–4566.
[53] L.P. Zhang, L. Zhu, L. Tang, et al., Adv. Sci. 10 (2022) 2205246.
[54] J. Gao, J. Li, W.C. Geng, et al., J. Am. Chem. Soc. 140 (2018) 4945–4953.
[55] J. Chen, Y. Zhang, Y. Zhang, et al., Chin. Chem. Lett. 32 (2021) 3034–3038.
[56] D.S. Guo, K. Wang, Y.X. Wang, Y. Liu, J. Am. Chem. Soc. 134 (2012) 10244–10250.
[57] M.E. Brewster, T. Loftsson, Adv. Drug Deliver Rev. 59 (2007) 645–666.
[58] A. Dahan, J.M. Miller, A. Hoffman, et al., J. Pharm. Sci. 99 (2010) 2739–2749.
[59] X. Ma, Y. Zhao, Chem. Rev. 115 (2015) 7794–7839.
[60] Z.X. Liu, Y. Liu, Chem. Soc. Rev. 51 (2022) 4786–4827.
[61] W.L. Zhou, W.J. Lin, Y. Chen, Y. Liu, Chem. Sci. 13 (2022) 7976–7989.
[62] S. Walker, R. Oun, F.J. McInnes, N.J. Wheate, Isr. J. Chem. 51 (2011) 616–624.
[63] S.J. Barrow, S. Kasera, M.J. Rowland, et al., Chem. Rev. 115 (2015) 12320–12406.
[64] W.L. Zhou, Y. Chen, Q.L. Yu, et al., Nat. Commun. 11 (2020) 4655.
[65] W.L. Zhou, Y. Chen, W. Lin, Y. Liu, Chem. Commun. 57 (2021) 11443–11456.
[66] S.B. Nimse, T. Kim, Chem. Soc. Rev. 42 (2013) 366–386.
[67] H. Zhang, Z. Liu, Y. Zhao, Chem. Soc. Rev. 47 (2018) 5491–5528.
[68] W. Feng, M. Jin, K. Yang, et al., Chem. Commun. 54 (2018) 13626–13640.
[69] M. Xue, Y. Yang, X.D. Chi, et al., Acc. Chem. Res. 45 (2012) 1294–1308.
[70] S.Y. Zhou, W.Z. Li, Q. Zhao, et al., ACS Appl. Mater. Interfaces 13 (2021) 58291–58300.
[71] M. Cen, Y. Ding, J. Wang, et al., ACS Macro Lett. 9 (2020) 1558–1562.
[72] Y. Cai, Z.C. Zhang, Y. Ding, et al., Chin. Chem. Lett. 32 (2021) 1267–1279.
[73] X.Y. Yu, Y. Chen, Chin. Chem. Lett. 34 (2023) 107739.
[74] Y.M. Zhang, Y.H. Liu, Y. Liu, Adv. Mater. 32 (2020) 1806158.
[75] X. Li, S. Zhou, Q. Zhao, et al., Angew. Chem. Int. Ed. (2023) e202216987.
[76] F.H. Lu, Y. Chen, B.Q. Fu, et al., Chin. Chem. Lett. 33 (2022) 5111–5115.
[77] S.Y. Zhou, Y. Chen, J. Xu, et al., J. Mater. Chem. B 11 (2023) 2706–2713.
[78] F.F. Shen, Y.M. Zhang, X.Y. Dai, et al., J. Org. Chem. 85 (2020) 6131–6136.
[79] W.J. Jin, Z.L. Chen, S.Y. Yang, et al., Chem. Commun. 58 (2022) 12584–12587.
[80] J. Liu, Y.Q. Xu, H.J. Lu, et al., Langmuir 38 (2022) 13955–13962.
[81] R. Bonnett, G. Martinez, Tetrahedron 57 (2001) 9513–9547.
[82] B. Jana, A.P. Thomas, S. Kim, et al., Chem. Eur. J. 26 (2020) 10695–10701.
[83] B. Yuan, H. Wu, H. Wang, et al., Angew. Chem. Int. Ed. 60 (2021) 706–710.